Faraday Discussions

Cite this: *Faraday Discuss.*, 2016, **194**, 259

PAPER

Novel photochemistry of molecular polaritons in optical cavities

Kochise Bennett,* Markus Kowalewski and Shaul Mukamel

Received 26th April 2016, Accepted 17th May 2016

DOI: 10.1039/c6fd00095a

Violations of the Born-Oppenheimer approximation (BOA) and the consequent nonadiabatic dynamics have long been an object of intense study. Recently, such dynamics have been induced *via* strong coupling of the molecule to a high-amplitude (spatially confined) mode of the electromagnetic field in optical cavities. However, the effects of a cavity on a pre-existing avoided crossing or conical intersection are relatively unexplored. The dynamics of molecules dressed by cavity modes are usually calculated by invoking the rotating wave approximation (RWA), which greatly simplifies the calculation but breaks down when the cavity mode frequency is higher than the relevant material frequencies. We develop a protocol for computing curve crossing dynamics in an optical cavity by exploiting a recently-developed method of solving the quantum Rabi model without invoking the RWA. The method is demonstrated for sodium iodide.

I. Introduction

The photochemistry of molecules can be significantly influenced by specially-tailored electromagnetic fields.[1–7] While control is usually described in terms of classical laser fields, coupling with the vacuum state of a cavity mode requires a quantum field description. The underlying theoretical framework, cavity quantum electrodynamics, has been well studied in theory and experiment with atoms.[8–10] Its application to molecular systems has been demonstrated recently with great success,[11,12] the dynamics being described using joint photon–matter states called polaritons. However, the inclusion of the internal nuclear degrees of freedom, not present in atomic systems, complicates the problem and leads to nonadiabatic dynamics.[13,14] The electric field mode alters the nuclear dynamics through its interaction with the electronic degrees of freedom, creating avoided curve crossings and conical intersections between the molecular potential energy surfaces. This can in principle be achieved by a strong laser field.[2,3] By placing the molecule in a localized cavity mode, a laser system is not necessary and the field can even be in the vacuum state. The former scenario can be described in terms of

---

Chemistry Department, University of California, Irvine, California 92697-2025, USA. E-mail: kcbennet@uci.edu

a classical field, while the latter requires a quantum field description. A major difference between the two scenarios is the number of photons available: a strong laser field may give rise to multi-photon pathways that may interfere with the intended control scheme.

A broad variety of photochemical and photophysical dynamics are controlled by naturally-occurring conical intersections (CIs) in the bare electronic-energy landscape, opening up fast, non-radiative relaxation pathways by which the molecule is funneled back to the ground state. In this contribution, we theoretically investigate how a molecule which already possesses a curve crossing is affected by coupling to a nano-scale cavity.

The Hamiltonian describing a two-level system linearly coupled to a quantized radiation field is given by the quantum Rabi model:

$$\hat{H} = \frac{\omega_0}{2}\left(2\hat{\sigma}^\dagger\hat{\sigma} - 1\right) + \omega_c\hat{a}^\dagger\hat{a} + \tilde{g}\left(\hat{a}^\dagger + \hat{a}\right)\left(\hat{\sigma}^\dagger + \hat{\sigma}\right) \tag{1}$$

where ω_0 is the energy difference between the exited state $|e\rangle$ and the ground state $|g\rangle$, $\hat{\sigma} = |g\rangle\langle e|$ is the annihilation operator for bare molecular excitations, and $\hat{a}^{(\dagger)}$ annihilates (creates) cavity-mode photons. The vacuum Rabi-frequency $\tilde{g} = \mu_{eg}\varepsilon_c\sqrt{n}$ determines the coupling strength between the photon mode and the molecular degrees of freedom. The vacuum field amplitude

$$\varepsilon_c = \sqrt{\frac{\omega_c}{V\varepsilon_0}} \tag{2}$$

is determined by the active mode volume V of the cavity mode, making nano-scale cavities favorable candidates to achieve strong coupling. The cavity coupling is further enhanced by a factor of $\sqrt{n}$ if an ensemble of n molecules contributes in a coherent fashion.

The approximations which can be used to find the eigenvalues of eqn (1) depend on the magnitude of $\tilde{g}$. Perturbative solutions are only possible for very small values of $\tilde{g}$, *i.e.*, much smaller than all other system frequencies. If the time scale of $\tilde{g}^{-1}$ is faster than the possible decay processes, we enter the strong coupling regime where the Jaynes–Cummings (JC) model[9] provides approximate solutions to the Hamiltonian (eqn (1)) in the form of dressed states. Formally, the JC model neglects the counter rotating terms ($\hat{\sigma}^\dagger\hat{a}^\dagger$ and $\hat{\sigma}\hat{a}$) in the Hamiltonian, a simplification called the Rotating Wave Approximation (RWA) which thus keeps only the $\hat{\sigma}^\dagger\hat{a} + \hat{\sigma}\hat{a}^\dagger$ term in the cavity–molecule coupling. In this case, the total excitation number $\hat{N} \equiv \hat{n}_c + \hat{\sigma}^\dagger\hat{\sigma}$ is a conserved quantity ($[\hat{N}, \hat{H}] = 0$), reducing the Hamiltonian to a 2-by-2 block-diagonal structure (see Fig. 1 upper panel). The bare states contributing to the dressed state basis are the ground state with n_c and $n_c + 1$ photons and the excited state with n_c photons. An extension to the JC model to include the nuclear degrees of freedom within the RWA has been reported recently.[13]

The RWA is justified in the regime of a weakly-driven system ($\tilde{g} \ll \omega_c$) and a reasonably-large transition frequency ($\omega_0/\omega_c > 0$). Both conditions are violated if we consider ultrastrong coupling to a molecule with a bare avoided crossing or CI. This case is the main focus of the present paper. As a result of this new parameter regime, the Hamiltonian acquires a band-diagonal structure as compared to a block diagonal structure (Fig. 1 upper panel). This Hamiltonian has been well-studied. Analytic expressions in terms of continued fractions were found by Judd

$$\left(\begin{array}{c:c:c:c} N_0 & & (a\sigma) & \\ \hdashline & \begin{pmatrix} N_1 \end{pmatrix} & & \ddots \\ \hdashline (a^\dagger\sigma^\dagger) & & \begin{pmatrix} N_2 \end{pmatrix} & \\ \hdashline & \ddots & & \ddots \end{array}\right)$$

$$\pi = +1: \; |g,0\rangle \rightarrow |e,1\rangle, |g,2\rangle \rightarrow |e,3\rangle, |g,4\rangle \rightarrow \ldots$$

$$\pi = -1: \; |e,0\rangle, |g,1\rangle \rightarrow |e,2\rangle, |g,3\rangle \rightarrow \ldots$$

Fig. 1 (Upper) Schematic depiction of the Hamiltonian. Under the RWA, $\hat{H}$ has a block-diagonal structure. Each block with a nonzero total excitation number is 2-by-2 and composed, in this basis, of $|e, n_c\rangle$, $|g, n_c + 1\rangle$. Adding back in the counter rotating terms couples states that differ by 2 in the total excitation number $\hat{N}$. (Lower) The simultaneous eigenstates of parity and excitation number. States with an even (odd) excitation number have even (odd) parity.

for an isolated set of eigenstates and the approach was further explicated in terms of the Bargmann representation and extended.[15–17] While a purely analytic, complete solution without the RWA is not possible, the problem has been treated in Fock space to allow for a numerically exact solution.[18,19] Operator methods have been discussed as well.[20,21]

The paper is organized as follows. In section B, we describe a semi-analytic method for solving the Schrödinger equation in the ultrastrong coupling regime. This method yields the potential energy surfaces of the coupled light-matter system and the nonadiabatic couplings between them. These will be used for the qualitative interpretation of the wavepacket simulations which are carried out using a numerical grid representation of the cavity mode as described recently.[22] In section IV, we discuss wavepacket simulation for sodium iodide in a cavity and show how the time-dependent branching ratio of the ionic and covalent configurations is manipulated in the presence of the cavity mode.

II. Nuclear motion through a nonadiabatic coupling region

We have recently discussed nuclear motion through a CI or avoided crossing (a region of nonadiabatic coupling) and the ways one may track this motion using spectroscopic signals.[13] We shall explore what occurs when such an experiment is performed in an electromagnetic cavity resonant with a material frequency (for some value of the nuclear coordinates). The system Hamiltonian is given by the sum of the nuclear kinetic energy operator $\hat{T}$ and the electronic Hamiltonian,

$$\hat{H} = \hat{T} + \hat{H}_{\text{el}} = -\frac{1}{2}\sum_{i=1}^{3N}\frac{1}{m_i}\nabla_i{}^2 + \sum_{l=1}^{l_{\text{M}}} \varepsilon_l(\mathbf{q})|\varepsilon_l(\mathbf{q})\rangle\langle\varepsilon_l(\mathbf{q})|. \tag{3}$$

The first term is the nuclear kinetic energy, where m_i is the mass of the i-th nuclear coordinate $\mathbf{q}_i$, $\nabla_i = \dfrac{\partial}{\partial \mathbf{q}_i}$ is the derivative with respect to $\mathbf{q}_i$, and we have explicitly notated the dependence of the electronic energies ε_l and corresponding eigenstates $|\varepsilon_l\rangle$ on the nuclear coordinates, collectively denoted $\mathbf{q}$. Taking the electronic matrix elements gives[23,24]

$$\hat{H}_{kl} = \delta_{kl}\left(\hat{T} + \varepsilon_l(\mathbf{q})\right) + \sum_i \frac{1}{m_i}\left(f_{kli}(\mathbf{q})\nabla_i + \frac{1}{2}h_{kli}(\mathbf{q})\right) \tag{4}$$

with

$$\begin{aligned} f_{kli}(\mathbf{q}) &= \langle \varepsilon_k(\mathbf{q})|\nabla_i|\varepsilon_l(\mathbf{q})\rangle \\ h_{kli}(\mathbf{q}) &= \langle \varepsilon_k(\mathbf{q})|{\nabla_i}^2|\varepsilon_l(\mathbf{q})\rangle. \end{aligned} \tag{5}$$

Given the electronic energies $\varepsilon_l(\mathbf{q})$, and the nonadiabatic couplings (NAC) $f_{kli}(\mathbf{q})$ and $h_{kli}(\mathbf{q})$, the total wavefunction may be written as a product of nuclear and electronic wavefunctions $|\Psi\rangle = |\phi\rangle|\psi\rangle = \sum_l c_l|\phi_l\rangle|\varepsilon_l\rangle$ where $|\phi_l\rangle$ is the nuclear wavepacket on the $|\varepsilon_l\rangle$ electronic surface and we have expanded the electronic wavefunction as a sum over eigenstates weighted by coefficients c_l. Any given initial state $|\Psi(t_0)\rangle$ can be propagated using the Hamiltonian eqn (4) to obtain the expectation values and correlation functions of material operators that are related to spectroscopic observables.

III. The quantum Rabi Hamiltonian

In Section II, we introduced the ingredients to the general Hamiltonian (eqn (4)) that we will use to propagate the nuclei. We now examine the quantum Rabi Hamiltonian (eqn (1)) in more detail. Taking matrix elements in the $\{|e\rangle, |g\rangle\}$ basis gives

$$H = \begin{pmatrix} \omega_c\hat{a}^\dagger\hat{a} - \dfrac{\omega_0}{2} & \tilde{g}\left(\hat{a}^\dagger + \hat{a}\right) \\ \tilde{g}\left(\hat{a}^\dagger + \hat{a}\right) & \omega_c\hat{a}^\dagger\hat{a} + \dfrac{\omega_0}{2} \end{pmatrix} \tag{6}$$

Switching to the basis $\left\{|+\rangle \equiv \dfrac{1}{\sqrt{2}}(|g\rangle + |e\rangle),\ |-\rangle \equiv \dfrac{1}{\sqrt{2}}(|g\rangle - |e\rangle)\right\}$ and dividing through by the cavity frequency (re-defining the unit of energy to be ω_c) gives

$$H = \begin{pmatrix} \hat{a}^\dagger\hat{a} + \dfrac{\tilde{g}}{\omega_c}\left(\hat{a}^\dagger + \hat{a}\right) & \dfrac{-\omega_0}{2\omega_c} \\ \dfrac{-\omega_0}{2\omega_c} & \hat{a}^\dagger\hat{a} - \dfrac{\tilde{g}}{\omega_c}\left(\hat{a}^\dagger + \hat{a}\right) \end{pmatrix} \tag{7}$$

which is a special (zero-bias) case of the model studied by[25] with parameters $g = \dfrac{\tilde{g}}{\omega_c}$, $\Delta = \dfrac{\omega_0}{\omega_c}$. This eigenvalue problem can be solved in a variety of ways. Numerical diagonalization using cavity field Fock states is possible but, for high values of g, requires that many states be taken into account (up to 10^5 at ultrastrong coupling depending on the convergence criteria[25]). Since our goal is to do non-BOA dynamics simulations, it is beneficial to use as few states as possible (this is particularly true for the calculation of the NAC). Using a Bargmann transformation and analyticity, Braak obtained a transcendental equation, the roots of which yield the energies, and this solution was later re-derived using extended coherent states.[21,26] The eigenstates and energies had also been derived earlier using tunable coherent states.[25] Both of these representations have an advantage over the Fock-space representations in that they automatically include many-body correlations amongst infinitely-many photons in the cavity mode. This is particularly useful in the strong coupling regime. Both of these representations have numerical difficulties when $g \ll 1$ but this regime is solvable within the RWA and can be smoothly connected provided we choose an appropriate separation point. More importantly, the former representation (extended coherent states) involves expressions that have periodic divergences, complicating numerical evaluation. For this reason, we choose to work in the basis of tunable, photon-added coherent states (*i.e.*, the basis of photon-added coherent states with a tunable coherence parameter) and make the ansatz

$$\begin{aligned}|\varepsilon\rangle_l &= |+\rangle \otimes \sum_{n=0}^{M} c_{nl}\left(\hat{a}^\dagger\right)^n e^{\alpha_l \hat{a}^\dagger}|0\rangle + \pi_l|-\rangle \otimes \sum_{n=0}^{M} c_{nl}\left(-\hat{a}^\dagger\right)^n e^{-\alpha_l \hat{a}^\dagger}|0\rangle \\ &= \begin{pmatrix} \sum_{n=0}^{M} c_{nl}(\hat{a}^\dagger)^n e^{\alpha_l \hat{a}^\dagger}|0\rangle \\ \pi_l \sum_{n=0}^{M} c_{nl}(-\hat{a}^\dagger)^n e^{-\alpha_l \hat{a}^\dagger}|0\rangle \end{pmatrix}\end{aligned} \tag{8}$$

where the c_{nl} coefficients represent the l-th eigenstate in the basis of n-photon-added tunable coherent states, α_l is the tunable coherent state parameter corresponding to the l-th eigenvalue, and $\pi_l = \pm 1$ is the parity of the l-th eigenstate. Since the Hamiltonian conserves the parity, we can separately consider the even and odd parity manifolds and write π_l explicitly rather than simply $\pm$ because we will later need to keep track of the two parities in the matrix elements $\langle \varepsilon_k | \hat{\mathcal{O}} | \varepsilon_l \rangle$ succinctly. In order that the π_l not be functions of the nuclear coordinates, we do not simply order the eigenstates by energy but rather list first the even and then the odd in ascending order of energy. In this ansatz, M is the truncation number. In practice, we must make M large enough to ensure convergence. This will be addressed in more detail later. Following the analysis of ref. 25 and inserting this wavefunction into the Schrödinger equation yields a connection between the energy and α_l

$$\varepsilon_l = \alpha_l g - \pi_l \frac{\Delta}{2} \tag{9}$$

and a recurrence relation for the coefficients

$$c_{n+1} = \frac{-c_0}{(n+1)g}\left[\left(n + \pi_l \frac{\Delta}{2}\right)c_n + (\alpha_l + g)c_{n-1} - \pi_l(-1)^n \frac{\Delta}{2}\sum_{j=0}^{n}\frac{(2\alpha_l)^j}{j!}c_{n-j}\right]. \tag{10}$$

Note that we have used $c_1 = 0$ (permitted since α_l can completely determine the 1-photon contribution to $|\varepsilon_l\rangle$) and that c_0 remains an arbitrary constant that can be used to normalize the states. This normalization and its consequences are discussed in detail in Appendix C but we will otherwise formally work with the normalized coefficients c_{nl}. Setting $c_{M+1} = 0$ (required for convergence) gives a degree M polynomial equation for α_l

$$\left(M + \pi_l \frac{\Delta}{2}\right) c_M + (\alpha_l + g) c_{M-1} - \pi_l (-1)^M \frac{\Delta}{2} \sum_{j=0}^{M} \frac{(2\alpha_l)^j}{j!} c_{M-j} = 0. \tag{11}$$

Chen *et al.*[25] had examined this recurrence relation for various regimes of the parameters Δ and g and we now briefly summarize their findings. For $0.1 < g < 0.5$ and $0.5 < \Delta < 1.5$, $M = 60$ is sufficient to ensure convergence (in the sense of a relative difference of 10^{-8} or less on increasing M further) for the first 20 or more eigenstates and the energies match those obtained *via* Fock state diagonalization (at a much higher truncation order). Moreover, the coefficients are found to die down by around $n = 40$ for $\Delta = 1, g = 0.1$ and this improves to $n = 10$ for $\Delta = 1, g = 1$. This shows the strength of this representation for handling the strong coupling regime. In the simulation section, we will discuss the parameters we used and the truncation.

Given a pair g, Δ, we can solve eqn (11) for the first N roots such that ε_N is sufficiently large to account for the system energetics. The details of this truncation will depend on the way in which the system is probed and the signal being examined.

It is worth repeating the findings of Braak[26] regarding the distribution of the zeroes of his G-function (not shown here for brevity) and thus, the energies. The zeroes of $G^{\pm}(x)$ are distributed relatively regularly, with the property that the number of eigenenergies in the range $[n\omega_c, (n+1)\omega_c]$ is restricted to be 0, 1, or 2. Additionally, two intervals each containing two eigenenergies will never be adjacent to each other (nor will two intervals each containing no eigenenergies). Since the G-function gives the exact energies as well, we are guaranteed that, for reasonably large ω_c, we will not have to include too many states $|\varepsilon_l\rangle$ to obtain converged calculations. This is trivially true for weak coupling at resonance ($g \ll 1$, $\Delta = 1$) but is good to confirm it for all parameter regimes.

In order to propagate an initial wavefunction so as to simulate spectra, we must obtain all the ingredients to compute $H_{kl}(\mathbf{q})$ in eqn (4). Besides the energies, we also need the nonadiabatic couplings $f_{kli}(\mathbf{q})$, and $h_{kli}(\mathbf{q})$. Computing these quantities is tedious but it is fairly straightforward. We outline the, rather lengthy, derivation in Appendix B and make frequent use of auxilliary quantities defined in Appendix A to arrive at

$$f_{kli} = f_{egi}(\pi_l - \pi_k) B_{kl}^{(1)} + (1 + \pi_k \pi_l)[A_{kl}^{(2)} + A_{kl}^{(3)} \nabla_i \alpha_l] \tag{12}$$

for the first-derivative couplings and

$$\begin{aligned} h_{kli} &= \nabla_i f_{kli} - F_{kli} \\ F_{kli} &= \frac{F_{gg} + F_{ee}}{2} \delta_{kl} + \frac{F_{gg} - F_{ee}}{2} (\pi_l + \pi_k) B_{kl}^{(1)} + F'_{eg} (1 - \pi_k \pi_l) A_{kl}^{(1)} \\ &\quad + \left[\left\{ f_{egi} (\pi_k - \pi_l) \left[B_{kl}^{(2)} - B_{kl}^{(3)} \nabla_i \alpha_l \right] \right\} + k \leftrightarrow l \right] \\ &\quad + (1 + \pi_k \pi_l) \left(A_{kl}^{(4)} \nabla_i \alpha_k + A_{lk}^{(4)} \nabla_i \alpha_l + A_{kl}^{(5)} \nabla_i \alpha_k \nabla_i \alpha_l + A_{kl}^{(6)} \right) \end{aligned} \tag{13}$$

for the second (we have suppressed the explicit $\mathbf{q}$-dependence for brevity).

IV. Application to avoided crossing in sodium iodide

The influence of ultrastrong cavity coupling is demonstrated on the nonadiabatic dynamics of photoexcited sodium iodide, a well known example for femtochemistry.[27] The adiabatic electronic states of the bare sodium iodide experience an avoided crossing near $\mathbf{q} \sim 8$ Å (Fig. 2(a)), leading to dissociation into the neutral products through the ^{1}X state upon photoexcitation. The bare nonadiabatic coupling matrix element f_{eg} is shown in Fig. 2(b). The branching ratio, *i.e.*, the amount of population transferred to the ^{1}X state, is determined by the acquired momentum of the wavepacket, which depends on the excitation laser frequency. We will investigate two scenarios: the cavity is set in resonance at ≈ 6 Å (case 1), *i.e.*, before the wavepacket in the A state reaches the bare avoided crossing, ($\omega_c =$ 815 meV) and a low frequency cavity ($\omega_c = 52.6$ meV) resonant directly at the crossing (case 2). Both cases are illustrated in Fig. 3 by plotting the ^{1}X-state curve shifted by the photon energy of the cavity.

For case 1, eqn (8) is used to calculate the resulting potential energy curves in the basis of the photon-added, tunable coherent states. Fig. 4 shows the lowest ten potential energy curves for four values of the coupling strength g. For small g,

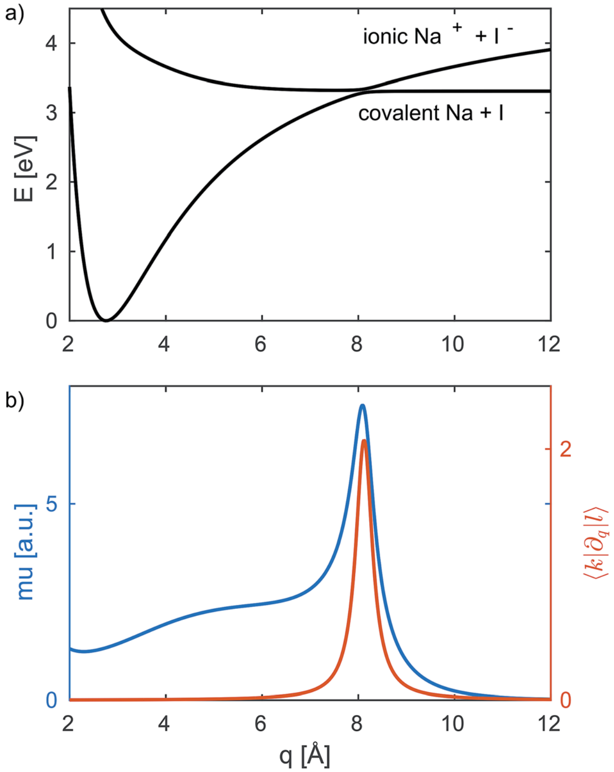

Fig. 2 (a) Bare ground (^{1}X) and excited (^{1}A) electronic potential energy surfaces of NaI. Dissociation on the ^{1}X potential leads to the neutral reaction products. (b) Transition dipole moment μ_{eg} (blue) and the derivative coupling matrix element f_{eg} (red).

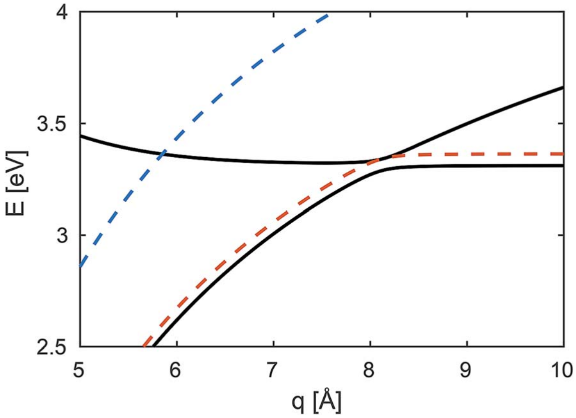

Fig. 3 Potential curve crossings for two different cavity detunings: ground state potential wavefunction shifted by the cavity frequency ($V_g + \omega_c$), for $\omega_c = 815$ meV (blue, dashed) and $\omega_c = 52.6$ meV (red, dashed).

the result converges to curves which coincide with a molecular Jaynes–Cummings model[13] (Fig. 4(a)). New avoided crossings are created in the region at 6 Å, where the cavity mode is in resonance with the bare electronic states of NaI ($\varDelta = 1$). New

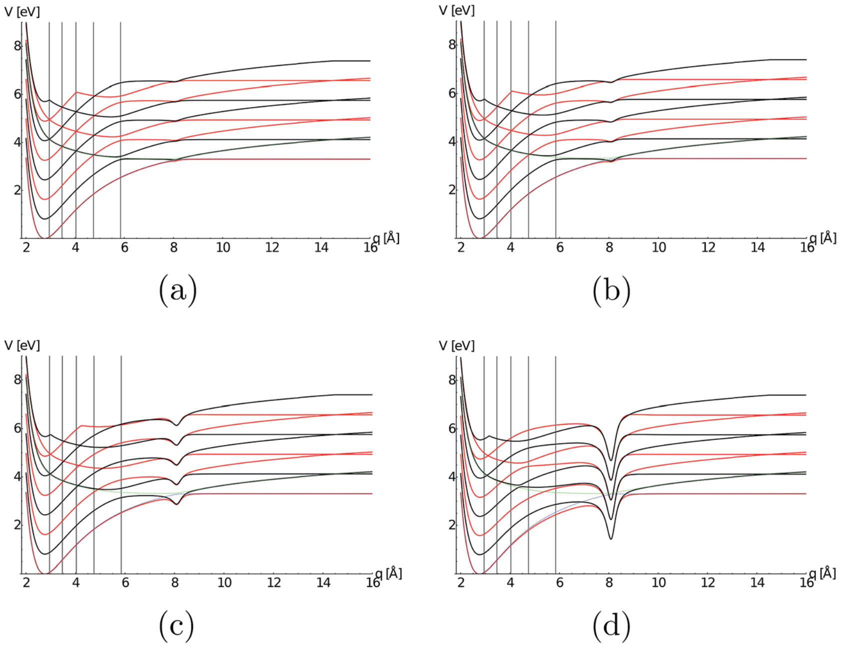

Fig. 4 Positive (red solid) and negative (black solid) parity electronic potential energy surfaces of NaI dressed with a $\omega_c = 815$ meV cavity mode obtained from eqn (9) and the first five solutions to eqn (11) with $\pi_l = +1$ and $\pi_l = -1$ respectively. Vertical gray lines indicate points where the bare states are resonant with integer multiples of the cavity frequency ($\omega_0 = n\omega_c$ for n an integer, $n = 1$ for the rightmost line and counts up going to the left). (a) Peak coupling of 200 meV. (b) Peak coupling of 300 meV. (c) Peak coupling of 600 meV. (d) Peak coupling of 1240 meV.

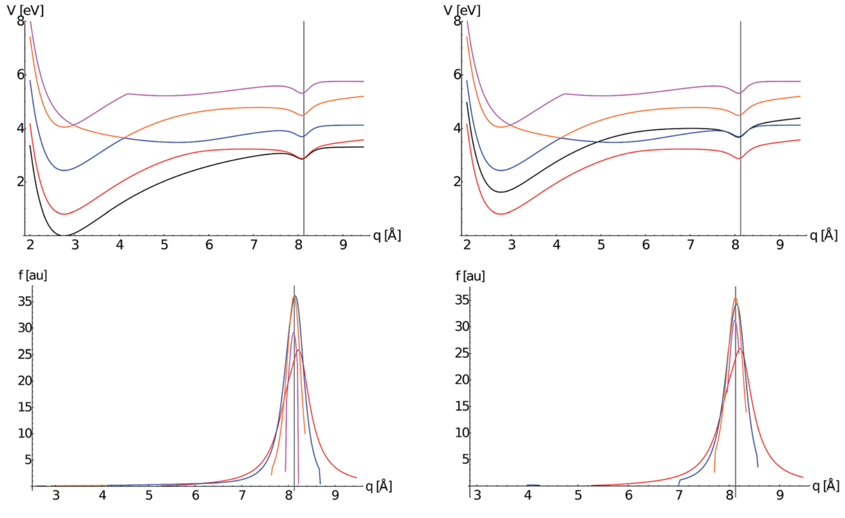

(a) (b)

Fig. 5 (a) Potential curves for the lowest energy positive-parity eigenstate (black) and the 4 lowest energy negative-parity eigenstates (upper) and their corresponding NACs (lower) (all couplings are between the "black" state and one of the others and therefore labeled by the color of the latter state). (b) Potential curves for the second-lowest positive-parity state (black) and the 4 lowest energy negative-parity eigenstates (upper) and their corresponding NACs (lower).

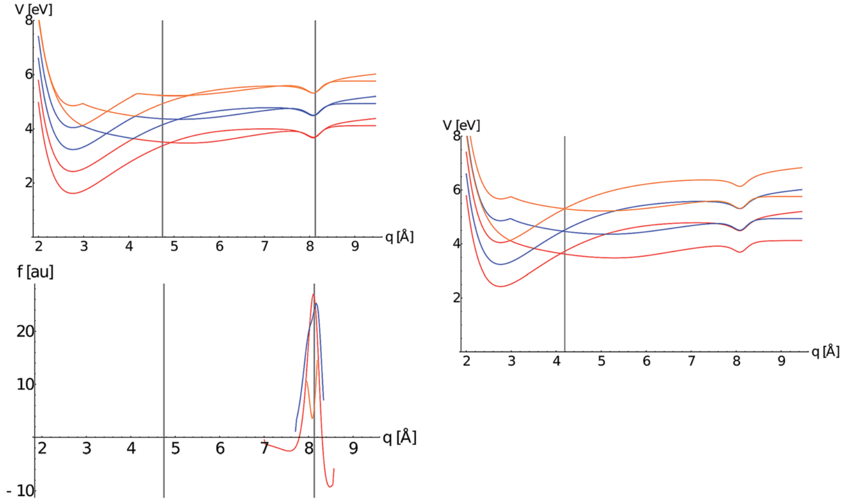

(a) (b)

Fig. 6 (a) Potential curves (upper) and corresponding NACs (lower) for 3 different pairs of opposite-parity eigenstates. (b) Potential curves for 3 different pairs of same-parity eigenstates. Corresponding NACs are sharply peaked at the avoided crossings near the gray line and are otherwise negligible.

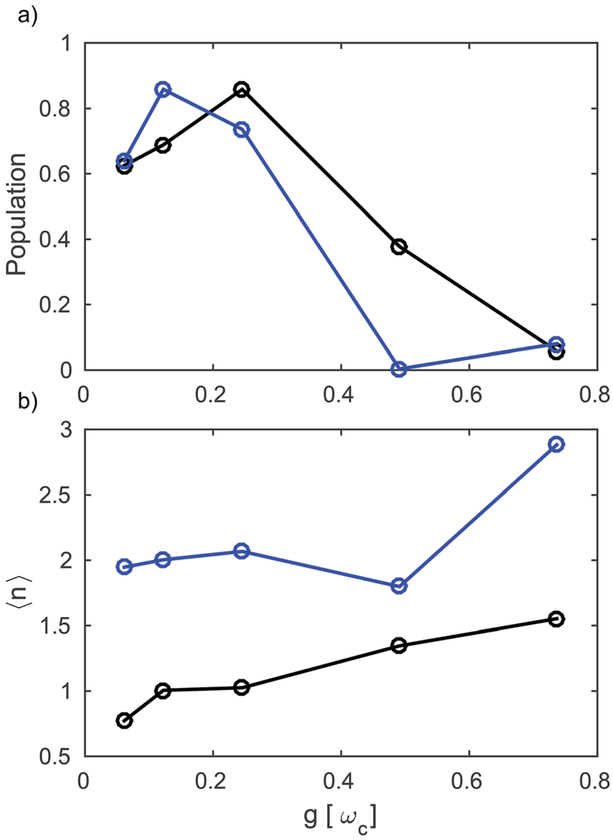

Fig. 7 Cavity coupling with $\omega_c = 815$ meV. (a) Population of the covalent states after 480 fs for a cavity with initially zero photons (black) and one photon (blue) *vs.* the coupling strength. (b) Average photon number 480 fs.

crossings are also created at higher-order resonances $\Delta = n$ between states of the same- (n odd) and opposite-parity (n even) states. As the coupling strength increases, the splitting between dressed states at the resonance points increases but it is much faster for lower-photon resonances. The splitting thus seems to depend inversely on n and directly on the absolute energy of the two states in question (with larger gaps for higher-energy pairs). Another notable feature is a ground-state modification[14,28] which becomes clearly visible with increasing coupling (Fig. 4). The dip is a clear signature of the ultrastrong coupling regime ($g \approx 1$). Fig. 5(a) shows the NACs (evaluated from eqn (12)) between the lowest positive-parity state (black) and the first 4 negative-parity states (energy surfaces in the upper panel and NACs in the lower panel). Fig. 5(b) shows the same but with the second-lowest positive-parity state). From this figure, it is clear that the NACs in the region of the original avoided crossing are strengthened relative to their bare values (Fig. 2 lower panel). Moreover, the coupling strength remains of the same order even for states separated by a large distance in energy. Fig. 6(a) shows the NACs between 3 pairs of opposite-parity states. Note that no NAC is induced in the region of crossing between such pairs (only the coupling in the

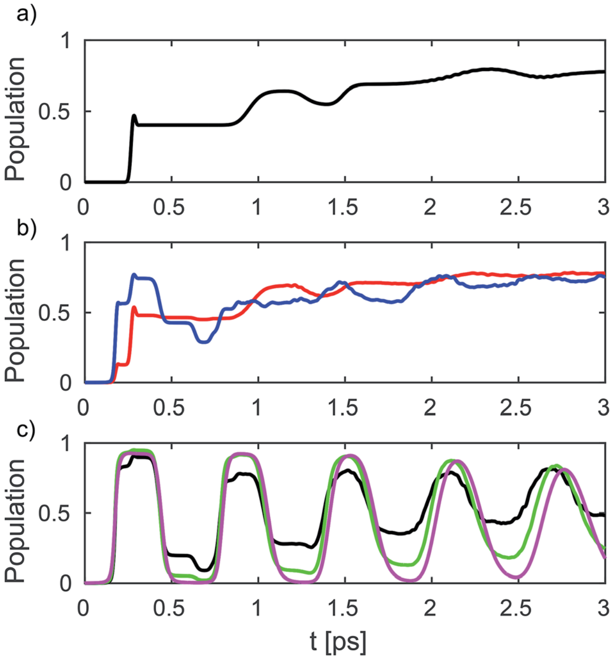

Fig. 8 Selected time traces of the ^{1}X state population (ω_c = 815 meV). No cavity (black line), g = (0.0502, 0.1256, 0.1884, 0.02512, 0.3793) red, blue, black, green, and magenta respectively.

region of the original avoided crossing remains). We can see that crossings between states of opposite parity do not generate any NACs. In contrast, the avoided crossings between states of the same parity correspond to peaks in the NAC curves. For a given resonance point (*e.g.*, $\omega_0 = 3\omega_c$), these peaks become smaller as one considers dressed states of higher energy (corresponding to larger separations at the avoided crossings).

To quantify the possible modifications of the dynamics under the influence of the cavity coupling, wavepacket calculations were carried out (for details see Appendix E). The amount of population in the dissociative part of the ^{1}X state after the wavepacket has reached the crossing point for the first time (≈480 fs) serves as an indicator of the effect on the dynamics. Fig. 7(a) depicts the population in the covalent channel for varying coupling strengths. While an intermediate coupling strength ($g < 0.3$) can increase the dissociation probability, the transfer to the ^{1}X state is suppressed for larger values of g. This behavior can be explained by the increased splitting between the dressed states: for larger splittings, the state which corresponds to the ^{1}A state is well-separated from the lower-lying state, effectively suppressing the population transfer.[13,14] The dynamics is mainly influenced by two modifications of the potential energy surfaces: the new avoided crossings created by the cavity and the modified avoided crossing already present in the bare molecule. With increasing cavity coupling, the cavity-created crossing at the 1-photon resonance point generates well-separated states such that a nuclear wavepacket is trapped and a much smaller fraction even reaches the original crossing. This partially coincides with the effect described by Galego

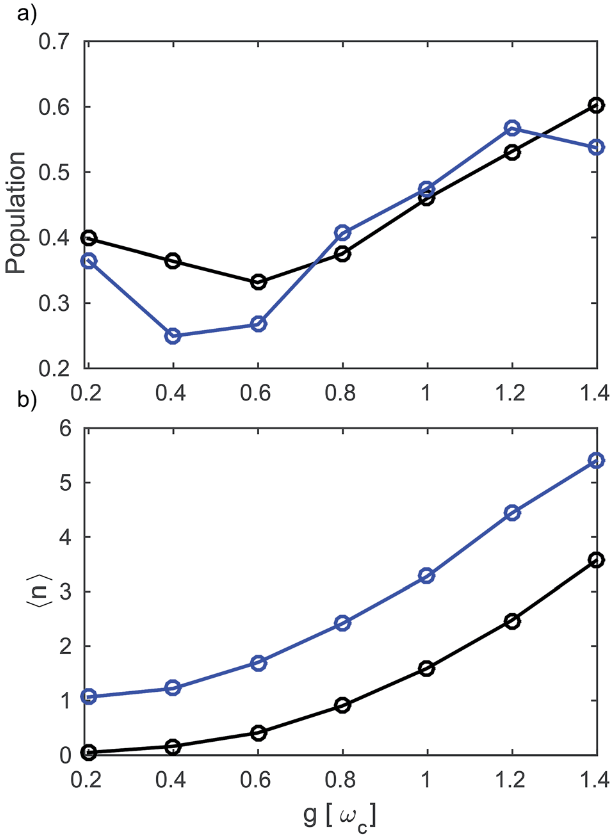

Fig. 9 (a) Population of the covalent states after 480 fs for a cavity with initially zero photons (black) and one photon (blue) *vs.* the coupling strength (ω_c = 52.6 meV). (b) Average photon number after 480 fs.

et al.[14] where for higher coupling strengths the states become well separated and the Born–Oppenheimer approximation is valid again. An alternative view is provided by the time evolution of the population of the ^{1}A state (Fig. 8). With increasing coupling strength, the wavepacket becomes trapped in a tighter effective potential and its recurrence time becomes shorter.

Additionally, both the NAC and the shape of the potential surface at the bare state avoided crossing is affected by the counter-rotating terms, creating a barrier for the nuclear wavepacket from which it reflects and allowing for further suppression of population transfer into the ^{1}X dissociation channel. The dissociation is strongly suppressed for large coupling strengths. The average photon number shown in Fig. 7 is a clear indicator that the system can not be represented by only two Fock states, but requires the present approach.

Case 2 is presented in Fig. 9. This case lacks an artificially-created avoided crossing at the 1-photon resonance point, thus simplifying the dynamics. The population in the X state after one round trip is shown in Fig. 9(a). The branching into the covalent state is slightly suppressed for small coupling strengths ($g < 0.6$) but increases for larger g. The increase in population transfer is accompanied by an increased number of photons (Fig. 9(b)) in the cavity mode, leading to the conclusion that stimulated emission into the cavity is the main mechanism for the control.

V. Discussion

Molecular cavity QED offers many exciting possibilities from enhanced probing techniques[12,29–33] to molecular cooling[34] and cavity-modified photochemistry.[13,35] The underlying Quantum Rabi model Hamiltonian is well-studied in the atomic context and has been solved in a number of ways.[9,15–18,20,21,25,26,36] In this work, we apply the solution in terms of tunable coherent states provided by Chen *et al.*[25] to the case of a molecular Hamiltonian with electronic parameters dependent on the nuclear configuration. We derive transformation formulas for electronic operators as well as expressions for the nonadiabatic coupling due to the nuclear kinetic-energy operator. Combined with the eigenstates, this is all the information necessary to carry-out and interpret dynamical simulations. By reducing the problem to familiar adiabatic energy surfaces and corresponding NACs, the dynamics can be understood even in non-intuitive parameter regimes. In particular, when a molecule possessing a CI or avoided crossing is dressed with an ultrastrong cavity field, the potential surfaces and NACs can be strongly modified from their bare or Jaynes–Cummings (RWA) shape.

Although the dynamics of a molecule interacting with a quantum field can be numerically solved in other ways, they possess limitations or do not provide the intuitive picture in terms of potential surfaces and NACs accessible here. Expansion in Fock-states (or the JC-polaritons) is the most straightforward approach but convergence is slow in the ultrastrong coupling regime ($g \sim 1$) and physical interpretation of the dynamics is complicated by the strong-mixing induced by the non-rotating terms in the Hamiltonian. Dynamical quantities can also be evaluated *via* discretization of the photon space as demonstrated recently[22] but the physical quantities that determine the evolution, the potential energy surfaces and NACs are never calculated in such a procedure and are thus inaccessible.

The method has been used to evaluate the photodissociation dynamics of sodium iodide as reproduced in Fig. 8. An analysis of the dynamics shows that, for small coupling, the population of the ^{1}X state increases in a step-wise fashion with time. Upon increasing the coupling, oscillations between the states are induced. These oscillations eventually die down to a nearly-even population. Examining the potential energy surfaces for increasing g (Fig. 4) reveals the opening of a gap at the 1-photon resonance ($\Delta \sim 1$) and the creation of a dip in the potential surface at the original avoided crossing while the NACs (Fig. 5) connect all pairs of opposite-parity states, providing decay paths to lower-energy pairs. For a nuclear wavepacket prepared in the ^{1}A state, these effects combine to create oscillations in the electronic populations, suppressing the final dissociation of the molecule.

The single-molecule coupling g is proportional to the vacuum field strength of the cavity mode given by

$$\varepsilon_c = \sqrt{\frac{\hbar\omega_c}{V\varepsilon_0}} = \sqrt{\frac{2\hbar\pi c}{\lambda_c V\varepsilon_0}} \tag{14}$$

where V is the mode volume of the cavity. The effective mode volumes used for the sodium iodide simulations range from $0.002\lambda_c{}^3$ to for $0.04\lambda_c{}^3$ for $\omega_c = 815$ meV and from $10^{-7}\lambda_c{}^3$ to for $10^{-5}\lambda_c{}^3$ for $\omega_c = 52.6$ meV for couplings present in Fig. 7 and 9 under the assumption that $\approx 10^5$ particles contribute collectively.[37] Nano-cavities,[38,39] nano-plasmon antennas,[40] or nano-guides[41] may provide a solution for the realization of such small effective mode volumes. Additionally, the collective enhancement effects must be leveraged to reach the ultrastrong coupling regime. In molecular systems however, these effects are subject to vibrational dephasing. Collective enhancement effects in molecules is a subject that needs further study and will be part of future investigations.

Appendix A

Working formulas for the tunable coherent-state basis

It is a known fact that eigenvectors corresponding to distinct eigenvalues are orthogonal. Thus, working with the normalized coefficients c_{nl}

$$\langle \varepsilon_k|\varepsilon_l\rangle = \delta_{kl}\langle \varepsilon_l|\varepsilon_l\rangle = \sum_{mn=0}^{M} c_{mk}c_{nl}\Big(\langle \alpha_k, m|\alpha_l, n\rangle + (-1)^{n+m}\pi_k\pi_l\langle -\alpha_k, m|-\alpha_l, n\rangle\Big) \quad \text{(A1)}$$

where

$$|\alpha_l, n\rangle \equiv (\hat{a}^{\dagger})^n e^{\alpha_l\hat{a}^{\dagger}}|0\rangle \quad \text{(A2)}$$

is the (un-normalized) n-photon-added coherent state with parameter α_l. For this orthogonality relation and for other purposes, we will need the quantity

$$\langle \alpha_k, m|\alpha_l, n\rangle = \sum_{pq=0}^{\infty}\left\langle q+m\left|\frac{\alpha_k{}^q\alpha_l{}^p\sqrt{q+m}\sqrt{p+n}}{q!p!}\right|p+n\right\rangle = \sum_{p=0}^{\infty}\frac{\alpha_l{}^p\alpha_k{}^{p+n-m}(p+n)!}{p!(p+n-m)!} \quad \text{(A3)}$$

This last formula is only valid for $n > m$ but, since all quantities in this overlap are real, it is symmetric with respect to the simultaneous exchange $k \leftrightarrow l$ and $n \leftrightarrow m$ so that this presents no difficulty. This form is convenient for seeing symmetries such as

$$\begin{aligned}\langle -\alpha_k, m|-\alpha_l, n\rangle &= (-1)^{n+m}\langle \alpha_k, m|\alpha_l, n\rangle\\ \langle \alpha_k, m|-\alpha_l, n\rangle &= (-1)^{n+m}\langle -\alpha_k, m|\alpha_l, n\rangle\end{aligned} \quad \text{(A4)}$$

and others that arise later in calculating the non-BOA couplings. For now, we use these relations to reduce the orthonormality condition to

$$\delta_{kl} = (1+\pi_k\pi_l)\sum_{mn=0}^{M} c_{mk}c_{nl}\langle \alpha_k, m|\alpha_l, n\rangle = (1+\pi_k\pi_l)A_{kl}^{(1)}(\mathbf{q}) \quad \text{(A5)}$$

where the last equality defines $A_{kl}^{(1)}$ which depends on $\mathbf{q}$ indirectly *via* the g and $\varDelta$. It is clear from the pre-factor that this condition is automatically satisfied for $\pi_k\pi_l = -1$, corresponding to states of opposite parity, while considering states of the same parity restricts $A_{kl}^{(1)}$ to vanish for $k \neq l$. The orthonormality condition also directly determines the initial coefficients c_{0l}. From eqn (10), (11), (A3) and

(A5), it is clear that it is not practical to solve it directly for the normalized coefficients c_{nl}. In practice, one must first solve it for a set of un-normalized coefficients using some other initial coefficient $\tilde{c}_{0l}$ (which we take to be 1 for all states) and then normalize after the fact. This will be discussed further in section C.

In calculating signals, we will be interested in evaluating expectation values or correlation functions of electronic operators such as the dipole or polarizability. The propagators in such an expression are easily evaluated *via* diagonalizing the truncated non-BOA Hamiltonian or a real-time propagation scheme. However, we will also need the operator matrix elements in the eigenbasis

$$\begin{aligned}\hat{\mathcal{O}}_{kl}(\mathbf{q}) &= \langle\varepsilon_k|\hat{\mathcal{O}}(\mathbf{q})|\varepsilon_l\rangle \\ &= \hat{\mathcal{O}}_{++}(\mathbf{q})\sum_{mn=0}^{M}c_{mk}c_{nl}\langle\alpha_k,m|\alpha_l,n\rangle + \hat{\mathcal{O}}_{--}(\mathbf{q})\pi_k\pi_l\sum_{mn=0}^{M}c_{mk}c_{nl}\langle\alpha_k,m|\alpha_l,n\rangle \\ &\quad + \hat{\mathcal{O}}_{+-}(\mathbf{q})\pi_l\sum_{mn=0}^{M}(-1)^n c_{mk}c_{nl}\langle\alpha_k,m|-\alpha_l,n\rangle \\ &\quad + \hat{\mathcal{O}}_{-+}(\mathbf{q})\pi_k\sum_{mn=0}^{M}(-1)^m c_{mk}c_{nl}\langle-\alpha_k,m|\alpha_l,n\rangle \end{aligned} \tag{A6}$$

where we have written the **q**-dependence for $\hat{\mathcal{O}}$ explicitly while omitting this dependence from the other variables (g and Δ and through them, the coefficients c_n as well as the α) for brevity. Defining the following summation

$$B_{kl}^{(1)}(\mathbf{q}) \equiv \sum_{mn=0}^{M}(-1)^n c_{mk}c_{nl}\langle\alpha_k,m|-\alpha_l,n\rangle, \tag{A7}$$

we obtain

$$\begin{aligned}\hat{\mathcal{O}}_{kl} = {} & \frac{\hat{\mathcal{O}}_{gg}+\hat{\mathcal{O}}_{ee}}{2}(1+\pi_k\pi_l)A_{kl}^{(1)} + \frac{\hat{\mathcal{O}}_{gg}-\hat{\mathcal{O}}_{ee}}{2}(\pi_k+\pi_l)B_{kl}^{(1)} + \Re\{\hat{\mathcal{O}}\}_{eg}(1-\pi_k\pi_l)A_{kl}^{(1)} \\ & + i\Im\{\hat{\mathcal{O}}_{eg}\}(\pi_l-\pi_k)B_{kl}^{(1)}\end{aligned} \tag{A8}$$

where we have suppressed the **q**-dependence for brevity. The $B_{kl}^{(1)}$ are complementary to the $A_{kl}^{(1)}$, differing only by the placement of the minus signs, and arise from cross terms between $|+\rangle$ and $|-\rangle$. Two particular operators are relevant for our purposes. The ionic state projection operator $|e\rangle\langle e| \equiv \hat{P}_e$ is given by

$$\left(\hat{P}_e\right)_{kl} = \frac{\delta_{kl}-(\pi_k+\pi_l)B_{kl}^{(1)}(\mathbf{q})}{2} \tag{A9}$$

and the transition dipole operator (or any operator with vanishing diagonal elements in the bare space) is given by

$$\begin{aligned}\hat{\mu}_{kl}(\mathbf{q}) = {} & \Re\{\hat{\mu}\}_{eg}(\mathbf{q})(1-\pi_k\pi_l)A_{kl}^{(1)}(\mathbf{q}) + i\Im\{\hat{\mu}\}_{eg}(\mathbf{q})(\pi_l-\pi_k)B_{kl}^{(1)}(\mathbf{q}) \rightarrow \hat{\mu}_{eg}(\mathbf{q}) \\ & (1-\pi_k\pi_l)A_{kl}^{(1)}\end{aligned} \tag{A10}$$

where the last relation is on the assumption of real transition dipole moments. We notice that this expression, whether real or complex, clearly vanishes for states of the same parity (as would be expected by the symmetry of the dipole operator). These two special cases correspond to the observables considered in the main text.

Appendix B

Derivation of the non-BOA couplings

To propagate nuclear wavepackets along the energy surfaces will require the non-BOA couplings f_{kli}, h_{kli}, which we obtain in this section. Since we will have frequent occasion to consider the derivative by the i-th nuclear coordinate, we notate such derivatives by a prime for brevity (*i.e.*, $\nabla_i[\ldots] \equiv [\ldots]'$ and there is no ambiguity since no terms mix nuclear derivatives) in the appendix. Using the expansion for the eigenstates (eqn (8)) and the product rules, we have

$$\begin{aligned} f_{kli} &= \langle \varepsilon_k|\nabla_i|\varepsilon_l\rangle \\ &= \langle +|\nabla_i|+\rangle A_{kl}^{(1)} + \langle -|\nabla_i|-\rangle \pi_k\pi_l A_{kl}^{(1)} + \langle +|\nabla_i|-\rangle \pi_l B_{kl}^{(1)} + \langle -|\nabla_i|+\rangle \pi_k B_{kl}^{(1)} \\ &\quad + (1+\pi_k\pi_l)\sum_{mn=0}^{M} c_{mk}c'_{nl}\langle \alpha_k, m|\alpha_l, n\rangle + \alpha'_l(1+\pi_k\pi_l)\sum_{mn=0}^{M} c_{mk}c_{nl}\langle \alpha_k, m|\alpha_l, n+1\rangle \end{aligned} \tag{B1}$$

where we have used $\nabla_i|\pm\alpha, n\rangle = \pm\alpha'|\pm\alpha, n+1\rangle$ and $\langle -\alpha_k, m|-\alpha_l, n+1\rangle = (-1)^{n+m+1}\langle \alpha_k, m|\alpha_l, n+1\rangle$, easily obtained from eqn (A2) and (A3). From basic considerations, $\langle e|\nabla_i|g\rangle = -\langle g|\nabla_i|e\rangle$ so that $\langle +|\partial_q|+\rangle = 0 = \langle -|\partial_q|-\rangle$ and the first two terms in the above vanish. The derivative coupling can then be easily written as

$$f_{kli} = \langle e|\nabla_i|g\rangle(\pi_l - \pi_k)B_{kl}^{(1)} + (1 + \pi_k\pi_l)[A_{kl}^{(2)} + \alpha'_l A_{kl}^{(3)}] \tag{B2}$$

where, for brevity, we have defined shorthand for two additional summations

$$\begin{aligned} A_{kl}^{(2)}(\mathbf{q}) &\equiv \sum_{mn=0}^{M} c_{mk}c'_{nl}\langle \alpha_k, m|\alpha_l, n\rangle \\ A_{kl}^{(3)}(\mathbf{q}) &\equiv \sum_{mn=0}^{M} c_{mk}c_{nl}\langle \alpha_k, m|\alpha_l, n+1\rangle. \end{aligned} \tag{B3}$$

The first term in eqn (B2) is simply the result of transforming a purely molecular-electronic operator with the appropriate symmetries and is thus proportional to the derivative coupling in the bare basis. The second term contains the two summations $A^{(2)}$ and $A^{(3)}$ which originate from the $\mathbf{q}$-derivative acting on the coefficients c_{nl} and the photonic state $|\alpha_l, n\rangle$ respectively.

To calculate the second-derivative coupling is somewhat more difficult but we can use the separation

$$h_{kli} = \langle \varepsilon_k|\nabla_i^2|\varepsilon_l\rangle = \nabla_i\langle \varepsilon_k|\nabla_i|\varepsilon_l\rangle - \langle \nabla_i\varepsilon_k|\nabla_i|\varepsilon_l\rangle = \nabla_i f_{kli} - F_{kli} \tag{B4}$$

where the last equality defines F_{kli} and the first term can be calculated numerically from the f_{kli} already obtained above. From

$$\begin{aligned} \nabla_i|\varepsilon_l\rangle = \sum_{n=0}^{M}\Big[&\nabla_i|+\rangle \otimes c_{nl}|\alpha_l, n\rangle + \pi_l\nabla_i|-\rangle \otimes (-1)^n c_{nl}|-\alpha_l, n\rangle + |+\rangle \otimes c'_{nl}|\alpha_l, n\rangle \\ &+ \alpha'_l|+\rangle \otimes c_{nl}|\alpha_l, n+1\rangle + \pi_l|-\rangle \otimes (-1)^n c'_{nl}|-\alpha_l, n\rangle \\ &- \alpha'_l\pi_l|-\rangle \otimes (-1)^n c_{nl}|-\alpha_l, n+1\rangle\Big] \end{aligned} \tag{B5}$$

it is straightforward, if somewhat tedious, to calculate the F_{kli}. It is convenient to separate the result into three terms

$$F_{kli} = \sum_{j=1}^{3} F_{kli}^{(j)} \tag{B6}$$

based on where the $\mathbf{q}$-derivatives (the ∇_i) act. The first term arises from transforming F from the $|e\rangle$, $|g\rangle$ basis as though it were an ordinary electronic operator

$$\begin{aligned} F_{kli}^{(1)} = {} & \frac{F_{gg} + F_{ee}}{2}(1 + \pi_k\pi_l)A_{kl}^{(1)} + \frac{F_{gg} - F_{ee}}{2}(\pi_l + \pi_k)B_{kl}^{(1)} + \Re\{F_{eg}\}(1 - \pi_k\pi_l)A_{kl}^{(1)} \\ & + i\Im\{F_{eg}\}(\pi_l - \pi_k)B_{kl}^{(1)}. \end{aligned} \tag{B7}$$

This is an unsurprising result and easily calculated from the bare F and the already-obtained $A^{(1)}$, $B^{(1)}$. The $F^{(1)}$ contribution can be thought of as collecting the terms in which both (of the two available) $\mathbf{q}$-derivatives act on the bare molecule states $|+\rangle$, $|-\rangle$ (due exclusively to the first two terms in eqn (B5)). The second term contributing to F_{kl} arises when only one $\mathbf{q}$-derivative acts on the bare molecular states, while the other acts on the coefficients c_{nl} or the photonic state $|\alpha_l, n\rangle$ (*i.e.*, cross terms between the first two and latter four elements of eqn (B5)). These contributions come as

$$F_{kli}^{(2)} = \{f_{egi}(\pi_k - \pi_l)[B_{kl}^{(2)} - \alpha'_l B_{kl}^{(3)}]\} + k \leftrightarrow l, \tag{B8}$$

where we have defined two more associated summations

$$\begin{aligned} B_{kl}^{(2)}(\mathbf{q}) &\equiv \sum_{mn=0}^{M} (-1)^n c_{mk} c'_{nl} \langle \alpha_k, m | -\alpha_l, n \rangle \\ B_{kl}^{(3)}(\mathbf{q}) &\equiv \sum_{mn=0}^{M} (-1)^n c_{mk} c_{nl} \langle \alpha_k, m | -\alpha_l, n + 1 \rangle \end{aligned} \tag{B9}$$

that again differ from their respective A summations only by the minus signs. These again arise as cross terms between $|+\rangle$ and $|-\rangle$ states with derivative operators intervening (directly leading to the matrix element f_{egi}). The final contribution to F_{kli} arises when both $\mathbf{q}$-derivatives act on coefficients or photonic states. There are several ways to distribute the derivative operations leading to

$$\begin{aligned} F_{kli}^{(3)} = {} & (1 - \delta_{kl})(1 + \pi_k\pi_l)(\alpha'_l A_{kl}^{(4)} + \alpha'_k A_{lk}^{(4)} \\ & + \alpha'_k \alpha'_l A_{kl}^{(5)} + A_{kl}^{(6)}) \end{aligned} \tag{B10}$$

where

$$\begin{aligned} A_{kl}^{(4)}(\mathbf{q}) &\equiv \sum_{mn=0}^{M} c'_{mk} c_{nl} \langle \alpha_k, m | \alpha_l, n + 1 \rangle \\ A_{kl}^{(5)}(\mathbf{q}) &\equiv \sum_{mn=0}^{M} c_{mk} c_{nl} \langle \alpha_k, m + 1 | \alpha_l, n + 1 \rangle \\ A_{kl}^{(6)}(\mathbf{q}) &\equiv \sum_{mn=0}^{M} c'_{mk} c'_{nl} \langle \alpha_k, m | \alpha_l, n \rangle \end{aligned} \tag{B11}$$

are the three relevant ways to distribute the two $\mathbf{q}$-derivatives between the coefficients and photon modes (the remaining conceivable combination does not contribute due to orthogonality) and the factor $(1 - \delta_{kl})$ is introduced to make clear that $F^{(3)}$ vanishes for diagonal elements (this can be shown analytically using the results of the following section).

Appendix C

Normalization

As mentioned briefly in Appendix A above, it is not practical to solve directly for the normalized coefficients c_{nl}. Instead, we recursively determine un-normalized coefficients $\tilde{c}_{nl}$ using the initial condition $\tilde{c}_{0l} = 1$ and then normalize afterwards. Thus, the normalization constant is

$$c_{0l} = \frac{1}{\sqrt{2\tilde{A}^{(1)}_{ll}(\mathbf{q})}} \tag{C1}$$

where the "tilde" indicates that the un-normalized coefficients $\tilde{c}_{nl}$ were used rather than the normalized c_{nl} as implied by eqn (A5) and we can clearly obtain

$$A^{(1)}_{kl} = \frac{\tilde{A}^{(1)}_{kl}}{2\sqrt{\tilde{A}^{(1)}_{kk}\tilde{A}^{(1)}_{ll}}} \equiv \overline{A}^{(1)}_{kl}. \tag{C2}$$

This last definition is superfluous for the $A^{(1)}$ summation but the consequences of a $\mathbf{q}$-dependent normalization will not always be quite so straightforward and defining the quantities

$$\overline{A}^{(j)}_{kl} = \frac{\tilde{A}^{(j)}_{kl}}{2\sqrt{\tilde{A}^{(1)}_{kk}\tilde{A}^{(1)}_{ll}}} \quad \overline{B}^{(j)}_{kl} = \frac{\tilde{B}^{(j)}_{kl}}{2\sqrt{\tilde{A}^{(1)}_{kk}\tilde{A}^{(1)}_{ll}}} \tag{C3}$$

facilitates compact expression of the correction terms. This straightforward normalization procedure only runs into difficulties when the $\mathbf{q}$-derivative of the coefficients c_{nl} are called for. As will become apparent from numerical implementation, the relative size of these coefficients spans many orders of magnitude, complicating numerical differentiation of the normalized coefficients. However, as we will show below, they can be obtained *via* a recurrence relation. We thus summarize the connections between normalized and un-normalized quantities

$$\begin{aligned}
A^{(j)}_{kl} &= \overline{A}^{(j)}_{kl}, \quad j = 1, 3, 5 \\
B^{(j)}_{kl} &= \overline{B}^{(j)}_{kl}, \quad j = 1, 3 \\
A^{(2)}_{kl} &= \overline{A}^{(2)}_{kl} - \left(\overline{A}^{(2)}_{ll} + \alpha'_l \overline{A}^{(3)}_{ll}\right)\overline{A}^{(1)}_{kl} \\
B^{(2)}_{kl} &= \overline{B}^{(2)}_{kl} - \left(\overline{A}^{(2)}_{ll} + \alpha'_l \overline{A}^{(3)}_{ll}\right)\overline{B}^{(1)}_{kl} \\
A^{(4)}_{kl} &= \overline{A}^{(4)}_{kl} - \left(\overline{A}^{(2)}_{kk} + \alpha'_k \overline{A}^{(3)}_{kk}\right)\overline{A}^{(3)}_{kl} \\
A^{(6)}_{kl} &= \overline{A}^{(6)}_{kl} - \left[\left(\overline{A}^{(2)}_{ll} + \alpha'_l \overline{A}^{(3)}_{ll}\right)\overline{A}^{(2)}_{lk} + k \leftrightarrow l\right] + \left(\overline{A}^{(2)}_{kk} + \alpha'_k \overline{A}^{(3)}_{kk}\right)\left(\overline{A}^{(2)}_{ll} + \alpha'_l \overline{A}^{(3)}_{ll}\right)\overline{A}^{(1)}_{kl}
\end{aligned} \tag{C4}$$

where we have used the readily-confirmed identity

$$\nabla_i \tilde{A}_{ll}^{(1)} = 2(\tilde{A}_{ll}^{(2)} + \alpha'_l \tilde{A}_{ll}^{(3)}) \tag{C5}$$

One can thus begin with the un-normalized coefficients $\tilde{c}_{nl}$ obtained from the initial condition $\tilde{c}_{0l} = 1$ and eqn (10) and (11). One can then normalize the coefficients c_{nl} *via* eqn (C1) and the amplitudes $\tilde{A}_{ll}^{(1)}$ before calculating all auxilliary summations directly from the c_{nl}. Alternatively, one can work with the un-normalized coefficients $\tilde{c}_{nl}$ and the un-normalized summations $\tilde{A}$ and $\tilde{B}$ can then be easily calculated and normalized afterwards *via* eqn (C4). However, to do this requires the nuclear derivative of the un-normalized coefficients, $\tilde{c}'_{nl}$. These can of course be obtained numerically but the better way is to take the derivative of the original recurrence relation to obtain

$$\begin{aligned} -g(n+1)\tilde{c}'_{n+1} = &-\left[(n+\pi_l)\frac{\varDelta}{2}\tilde{c}'_n + (\alpha_l+g)\tilde{c}'_{n-1} - \pi_l(-1)^n\frac{\varDelta}{2}\sum_{j=0}^{n}\frac{(2\alpha_l)^j}{j!}\tilde{c}'_{n-j}\right] \\ &+ (n+1)\tilde{c}_{n+1}\left(g' - g\frac{\varDelta'}{\varDelta}\right) + n\tilde{c}_n\left(2g\alpha'_l - \frac{\varDelta}{\varDelta}\right) + \tilde{c}_{n-1} \\ &\times\left(g' + \alpha'_l(2n-1+\varDelta\pi_l) - \frac{\varDelta'}{\varDelta}(\alpha_l+g)\right) + 2\alpha_l\tilde{c}_{n-2}(\alpha_l+g) \end{aligned} \tag{C6}$$

where we have used the original recursion relation to simplify the result. The derivatives of coefficients then depend only on the g, $\varDelta$, α, which are already available, and their derivatives g', $\varDelta'$, α', the former two of which can be obtained numerically while the latter can be obtained self-consistently from the truncation relation (*i.e.*, setting $\tilde{c}'_M = 0$). In this paper, we take this latter approach to avoid numerically differentiating the coefficients.

Appendix D

Summary of formulas

In this section, we summarize the final formulas obtained for all key quantities. Namely, the following table summarizes the various summations necessary for the transformation of electronic operators and the calculation of the derivative couplings. For brevity, we have omitted the summation symbol $\sum_{mn}^{M}$ from the

Table 1 Summary of direct ($A_{kl}^{(i)}$) and complementary cross term ($B_{kl}^{(i)}$) summations used as auxilliary quantities to obtain operator matrix elements $\mathscr{O}_{kl}$ and non-BOA coupling f_{kli} and F_{kli} coming from first- and second-derivative couplings respectively

i	$A_{kl}^{(i)}$	$B_{kl}^{(i)}$	Type of terms
1	$c_{mk}c_{nl}\langle\alpha_k, m\|\alpha_l, n\rangle$	$(-1)^n c_{mk}c_{nl}\langle\alpha_k, m\|-\alpha_l, n\rangle$	Zero-derivative direct and cross terms
2	$c_{mk}c'_{nl}\langle\alpha_k, m\|\alpha_l, n\rangle$	$(-1)^n c_{mk}c'_{nl}\langle\alpha_k, m\|-\alpha_l, n\rangle$	One-derivative direct and cross terms
3	$c_{mk}c_{nl}\langle\alpha_k, m\|\alpha_l, n+1\rangle$	$(-1)^n c_{mk}c_{nl}\langle\alpha_k, m\|-\alpha_l, n+1\rangle$	
4	$c'_{mk}c_{nl}\langle\alpha_k, m\|\alpha_l, n+1\rangle$		Two-derivative direct terms
5	$c_{mk}c_{nl}\langle\alpha_k, m+1\|\alpha_l, n+1\rangle$		
6	$c'_{mk}c'_{nl}\langle\alpha_k, m\|\alpha_l, n\rangle$		

entries of columns two and three. The photon-added coherent state overlaps are given by eqn (A3) which may be recast as

$$\langle \alpha_k, m|\alpha_l, n\rangle = {}_1F_1(1+n, 1+n-m, \alpha_k\alpha_l){\alpha_l}^{n-m}(n)_m \tag{D1}$$

where $(n)_m = n(n-1)(n-(m-1))$ is the falling factorial and ${}_1F_1(a, b, c)$ is the Kummer confluent hypergeometric function. This form is particularly useful for numeric implementation. The un-normalized coefficients $\tilde{c}_{nl}$ are given as polynomials in α by the recurrence relation eqn (10) with $\tilde{c}_{0l} = 1$. After solving eqn (11), we obtain the α_l, and thus the $\tilde{c}_{nl}$, numerically. The sums given in Table 1 can then be calculated and used to evaluate the three key quantities necessary for evaluation of signals (transformed electronic operators, and first and second derivative couplings), which we write here in terms of the easily calculated "tilde" and "bar" quantities for completion

$$\begin{aligned}
\hat{\mathcal{O}}_{kl} ={}& \frac{\hat{\mathcal{O}}_{gg}+\hat{\mathcal{O}}_{ee}}{2}(1+\pi_k\pi_l)\overline{A}_{kl}^{(1)} + \frac{\hat{\mathcal{O}}_{gg}-\hat{\mathcal{O}}_{ee}}{2}(\pi_k+\pi_l)\overline{B}_{kl}^{(1)} + \Re\{\hat{\mathcal{O}}_{eg}\}(1-\pi_k\pi_l)\overline{A}_{kl}^{(1)} \\
&+ i\Im\{\hat{\mathcal{O}}_{eg}\}(\pi_l-\pi_k)\overline{B}_{kl}^{(1)} \\
f_{kli} ={}& f_{egi}(\pi_l-\pi_k)\overline{B}_{kl}^{(1)} + (1+\pi_k\pi_l)\left[\overline{A}_{kl}^{(2)} - \overline{A}_{ll}^{(2)}\overline{A}_{kl}^{(1)} + \alpha'_l\left(\overline{A}_{kl}^{(3)} - \overline{A}_{ll}^{(3)}\overline{A}_{kl}^{(1)}\right)\right] \\
F_{kli} ={}& \frac{F_{gg}+F_{ee}}{2}\delta_{kl} + \frac{F_{gg}-F_{ee}}{2}(\pi_l+\pi_k)\overline{B}_{kl}^{(1)} + F'_{eg}(1-\pi_k\pi_l)\overline{A}_{kl}^{(1)} + f_{egi}(\pi_k-\pi_l) \\
&\times\left[\left\{\left[\overline{B}_{kl}^{(2)} - \alpha'_l\overline{B}_{kl}^{(3)}\right] - \left(\overline{A}_{ll}^{(2)} + \alpha'_l\overline{A}_{ll}^{(3)}\right)\overline{B}_{kl}^{(1)}\right\} + k\leftrightarrow l\right] + (1-\delta_{kl})(1+\pi_k\pi_l) \\
&\times\Bigg[\left(\alpha'_l\overline{A}_{kl}^{(4)} + \alpha'_k\overline{A}_{lk}^{(4)} + \alpha'_k\alpha'_l\overline{A}_{kl}^{(5)} + \overline{A}_{kl}^{(6)}\right) \\
&+\left(\left(\overline{A}_{kk}^{(2)} + \alpha'_k\overline{A}_{kk}^{(3)}\right)\left(\overline{A}_{kl}^{(2)} + \overline{A}_{kl}^{(3)}\right) + k\leftrightarrow l\right) + A_{kl}^{(1)}\left(\overline{A}_{ll}^{(2)} + \alpha'_l\overline{A}_{ll}^{(3)}\right)^2\Bigg]
\end{aligned} \tag{D2}$$

Appendix E

Direct space quantization of the photonic degrees of freedom

The analytical diagonalization of the matter-field Hamiltonian as described in this paper yields a set of new potential energy surfaces and nonadiabatic couplings. This representation provides an intuitive picture and insight into the modified structure of the coupled Hamiltonian but might become intractable for a quantum dynamics time propagation. An alternative efficient computational scheme is obtained by the direct treatment of the cavity mode[22] in analogy to the quantum harmonic oscillator. The annihilation and creation operators of the cavity mode can be expressed in terms their quadrature coordinates x and p:

$$a = \sqrt{\frac{\omega_c}{2\hbar}}\left(\hat{x} + \frac{i}{\omega_c}\hat{p}\right) \tag{E1}$$

The coupled light-molecule Hamiltonian from eqn (1) then reads:

$$H = \frac{\omega_0}{2}\left(2\hat{\sigma}^\dagger\hat{\sigma} - 1\right) - \frac{\hbar}{2}\frac{\partial^2}{\partial x^2} + \frac{1}{2}{\omega_c}^2\hat{x}^2 + \tilde{g}\sqrt{2\hbar\omega_c}\hat{x}\left(\hat{\sigma}^\dagger + \hat{\sigma}\right) \tag{E2}$$

The coordinate X is treated as a spatial coordinate, putting the nuclear coordinates and the cavity mode on an equal footing in a numerical simulation. Here x is discretized on a numerical grid and the second derivative with respect to x can then be conveniently calculated by a discrete Fourier transform.[42] The nuclear degrees of freedom $\mathbf{q}$ are accounted for by treating ω_0 and $\tilde{g}$ as functions of $\mathbf{q}$ (*i.e.* the potential energy curves and transition dipole curves respectively).

The wavepacket simulations have been carried out by propagating the photonic-nuclear wave packet on the potential energy curves of NaI (^{1}X and ^{1}A) using the Hamiltonian from eqn (E2). The time stepping was done with a Chebychev propagation scheme.[43] The potential energy curves NaI, as well as the nonadiabatic coupling matrix element and the transition dipole moment has been calculated with the program package MOLPRO[44] at the MRCI/CAS(6/7)/aug-cc-VQZ level of theory with an effective core potential for iodine (ECP46MWB).

Appendix F

Simulation protocol

Below, we outline the necessary steps to implementing the calculation of a time-dependent signal that tracks the evolving nuclear wavepacket on the multitude of electronic energy surfaces.

1. Obtain eigenenergies ε_l of the electronic Hamiltonian

(a) Obtain $g(\mathbf{q})$, $\Delta(\mathbf{q})$ from quantum chemistry and definitions.

(b) Discretize $\mathbf{q}$-space on a multidimensional grid.

(c) For each point in $\mathbf{q}$-space, obtain the first N solutions, $\alpha_1 \cdots \alpha_N$, of eqn (11) with $\varepsilon = \alpha g - \pi \dfrac{\Delta}{2}$ sufficiently large for the problem (this depends on the type of signal being discussed).

2. Transform electronic operators to eigenbasis

(a) For each $\varepsilon_l(\mathbf{q})$, use eqn (10) to obtain the coefficients $c_{nl}(\mathbf{q})$ of the eigenstate expansions.

(b) For each $\mathbf{q}$-point, use eqn (A2) and the α_l from step 1(c) above to obtain the photon-state overlaps $\langle \alpha_k, m | \alpha_l, n \rangle$ and $\langle \alpha_k, m | -\alpha_l, n \rangle$ for all choices of $k, l \in \{1,\ldots, N\}$ and $m, n \in \{1,\ldots, M\}$. This is two sets of $(NM)^2$ quantities.

(c) Use the coefficients c_{nl} and the photon-state overlaps $\langle \alpha_k, m | \alpha_l, n \rangle$ and $\langle -\alpha_k, m | \alpha_l, n \rangle$ to calculate the summations $A_{kl}^{(1)}(\mathbf{q})$, $B_{kl}^{(1)}(\mathbf{q})$ *via* eqn (A7)

(d) Use eqn (A8) to transform any electronic operator. Special cases include the ionic-state population operator (eqn (A9)) and the transition dipole operator (eqn (A10)).

3. Obtain the derivative couplings $f_{kli}(\mathbf{q})$

(a) Obtain the derivative couplings for the bare molecule, $f_{egi}(\mathbf{q})$, from quantum chemistry calculations.

(b) Take numeric derivatives of the $\alpha_l(\mathbf{q})$ and $c_{nl}(\mathbf{q})$ obtained above with respect to the nuclear coordinates to obtain the quantities $\alpha'_l(\mathbf{q})$ and $c'_{nl}(\mathbf{q})$.

(c) Using $c'_{nl}(\mathbf{q})$ and eqn (B3), calculate the summations $A_{kl}^{(2,3)}(\mathbf{q})$.

(d) Using $\alpha'_l(\mathbf{q})$, $f_{egi}(\mathbf{q})$ and the auxiliary summations, calculate $f_{kli}(\mathbf{q})$ *via* eqn (12).

4. Obtain second-derivative couplings $h_{kli}(\mathbf{q})$

(a) Use eqn (B4) to recast the problem into finding $F_{kli}(\mathbf{q}) \equiv \langle \nabla_i \varepsilon_k | \nabla_i \varepsilon_l \rangle (\mathbf{q})$.

(b) Obtain matrix elements of F for the bare molecule (F_{gg}, F_{ee}, F_{eg}) from quantum chemistry calculations.

(c) Calculate auxiliary summations $A_{kl}^{(j)}, j \in \{4, 5, 6\}$.

(d) Assemble F_{kli} *via* eqn (13).

5. Calculate desired signals

(a) Write the desired signal in terms of expectation values or correlation functions of electronic operators.

(b) Write the Hamiltonian in the form of eqn (4) with $\varepsilon_l(\mathbf{q})$, $f_{kli}(\mathbf{q})$ and $h_{kli}(\mathbf{q})$ are given by steps 1, 3, and 4 above.

(c) Using this Hamiltonian and some time propagation scheme (such as the Short-Iterative Lanczos time-stepping procedure), any initial state can be propagated in time.

(d) The action of electronic operators in this basis can be computed using the results of step 2 above.

(e) Combining these two ingredients, we can calculate any expectation value or correlation function of electronic operators.

(f) Convolutions of these expectation values or correlation functions with external field envelopes then give the observable signal of interest.

Acknowledgements

The support of the National Science Foundation (grant CHE-1361516) as well as from the Chemical Sciences, Geosciences, and Biosciences division, Office of Basic Energy Sciences, Office of Science, U.S. Department of Energy through award No. DE-FG02-04ER15571, is gratefully acknowledged. The computational resources and support for K. B. was provided by DOE. M. K. gratefully acknowledges support from the Alexander von Humboldt foundation through the Feodor Lynen program. We would like to thank the green planet cluster (NSF Grant CHE-0840513) for allocation of compute resources.

References

1 P. V. Demekhin and L. S. Cederbaum, *J. Chem. Phys.*, 2013, **139**, 154314.
2 J. Kim, H. Tao, J. L. White, V. S. Petrović, T. J. Martinez and P. H. Bucksbaum, *J. Phys. Chem. A*, 2012, **116**, 2758.
3 P. von den Hoff, M. Kowalewski and R. de Vivie-Riedle, *Faraday Discuss.*, 2011, **153**, 159.
4 P. von den Hoff, S. Thallmair, M. Kowalewski, R. Siemering and R. de Vivie-Riedle, *Phys. Chem. Chem. Phys.*, 2012, **14**, 14460.
5 P. Gross, D. Neuhauser and H. Rabitz, *J. Chem. Phys.*, 1992, **96**, 2834.
6 P. Brumer and M. Shapiro, *Chem. Phys. Lett.*, 1986, **126**, 541.
7 D. J. Tannor, R. Kosloff and S. A. Rice, *J. Chem. Phys.*, 1986, **85**, 5805.
8 E. M. Purcell, *Phys. Rev.*, 1946, **69**, 674.
9 E. T. Jaynes and F. W. Cummings, *Proc. IEEE*, 1963, **51**, 89.
10 S. Haroche and J.-M. Raimond, *Exploring the Quantum: Atoms, Cavities, and Photons (Oxford Graduate Texts)*, 1st edn, Oxford University Press, 2006.
11 J. A. Hutchison, T. Schwartz, C. Genet, E. Devaux and T. W. Ebbesen, *Angew. Chem., Int. Ed.*, 2012, **51**, 1592.

12 A. Shalabney, J. George, H. Hiura, J. A. Hutchison, C. Genet, P. Hellwig and T. W. Ebbesen, *Angew. Chem., Int. Ed.*, 2015, **54**, 7971.

13 M. Kowalewski, K. Bennett and S. Mukamel, *J. Chem. Phys.*, 2016, **144**, 054309.

14 J. Galego, F. J. Garcia-Vidal and J. Feist, *Phys. Rev. X*, 2015, **5**, 041022.

15 B. Judd, *J. Phys. C: Solid State Phys.*, 1979, **12**, 1685.

16 H. Reik, H. Nusser and L. A. Ribeiro, *J. Phys. A: Math. Gen.*, 1982, **15**, 3491.

17 M. Kus and M. Lewenstein, *J. Phys. A: Math. Gen.*, 1986, **19**, 305.

18 S. Swain, *J. Phys. A: Math. Gen.*, 1973, **6**, 1919.

19 S. He, C. Wang, Q.-H. Chen, X.-Z. Ren, T. Liu and K.-L. Wang, *Phys. Rev. A*, 2012, **86**, 033837.

20 I. D. Feranchuk, L. I. Komarov and A. P. Ulyanenkov, *J. Phys. A: Math. Gen.*, 1996, **29**, 4035.

21 Q.-H. Chen, C. Wang, S. He, T. Liu and K.-L. Wang, *Phys. Rev. A*, 2012, **86**, 023822.

22 M. Kowalewski, K. Bennett and S. Mukamel, *J. Phys. Chem. Lett.*, 2016, **7**, 2050–2054.

23 A. Hofmann and R. de Vivie-Riedle, *Chem. Phys. Lett.*, 2001, **346**, 299.

24 W. Domcke, D. R. Yarkony and H. Köppel, *Conical Intersections*, WORLD SCIENTIFIC, 2011, vol. 17.

25 Q.-H. Chen, T. Liu, Y.-Y. Zhang and K.-L. Wang, *Europhys. Lett.*, 2011, **96**, 14003.

26 D. Braak, *Phys. Rev. Lett.*, 2011, **107**, 100401.

27 A. Mokhtari, P. Cong, J. L. Herek and A. H. Zewail, *Nature*, 1990, **348**, 225.

28 T. Liu, K.-L. Wang and M. Feng, *J. Phys. B: At., Mol. Opt. Phys.*, 2007, **40**, 1967.

29 F. C. Spano, *J. Chem. Phys.*, 2015, **142**, 184707.

30 F. Caruso, S. K. Saikin, E. Solano, S. F. Huelga, A. A. Guzik and M. B. Plenio, *Phys. Rev. B*, 2012, **85**, 125424.

31 P. Saurabh and S. Mukamel, *J. Chem. Phys.*, 2016, **144**, 124115.

32 J. del Pino, J. Feist and F. J. Garcia-Vidal, *J. Phys. Chem. C*, 2015, **119**, 29132.

33 B. S. Simpkins, K. P. Fears, W. J. Dressick, B. T. Spann, A. D. Dunkelberger and J. C. Owrutsky, *ACS Photonics*, 2015, **2**, 1460.

34 M. Kowalewski, G. Morigi, P. W. H. Pinkse and R. de Vivie Riedle, *Phys. Rev. A*, 2011, **84**, 033408.

35 F. Herrera and F. C. Spano, *Cavity-controlled Chemistry in Molecular Ensembles*, 2015, arXiv:1512.05017.

36 J. Casanova, G. Romero, I. Lizuain, J. J. García-Ripoll and E. Solano, *Phys. Rev. Lett.*, 2010, **105**, 263603.

37 T. Schwartz, J. A. Hutchison, J. Léonard, C. Genet, S. Haacke and T. W. Ebbesen, *ChemPhysChem*, 2013, **14**, 125.

38 S. Tomljenovic-Hanic, M. J. Steel, C. M. de Sterke and J. Salzman, *Opt. Express*, 2006, **14**, 3556–3562.

39 A. D. Greentree, C. Tahan, J. H. Cole and L. C. L. Hollenberg, *Nat. Phys.*, 2006, **2**, 856, arXiv:cond-mat/0609050.

40 M.-K. Kim, H. Sim, S. J. Yoon, S.-H. Gong, C. W. Ahn, Y.-H. Cho and Y.-H. Lee, *Nano Lett.*, 2015, **15**, 4102.

41 S. Faez, P. Türschmann, H. R. Haakh, S. Götzinger and V. Sandoghdar, *Phys. Rev. Lett.*, 2014, **113**, 213601.

42 D. J. Tannor, *Introduction to Quantum Mechanics: a Time-dependent Perspective*, University Science Books.

43 H. T. Ezer and R. Kosloff, *J. Chem. Phys.*, 1984, **81**, 3967.

44 H.-J. Werner, P. J. Knowles, G. Knizia, F. R. Manby and M. Schütz, *et al.*, *Molpro, Version 2015.1*, a package of ab initio programs, 2015, see http://www.molpro.net.